Local Spectroscopy of the Electrically Tunable Band Gap in Trilayer Graphene

Matthew Yankowitz,[1] Fenglin Wang,[2] Chun Ning Lau,[2] and Brian J. LeRoy[1,*]

[1] *Physics Department, University of Arizona, 1118 E 4th Street, Tucson, AZ 85721, USA*

[2] *Department of Physics and Astronomy, University of California, Riverside, CA 92521, USA*

(Dated: January 14, 2013)

Abstract

The stacking order degree of freedom in trilayer graphene plays a critical role in determining the existence of an electric field tunable band gap. We present spatially-resolved tunneling spectroscopy measurements of dual gated Bernal (ABA) and rhombohedral (ABC) stacked trilayer graphene devices. We demonstrate that while ABA trilayer graphene remains metallic, ABC trilayer graphene exhibits a widely tunable band gap as a function of electric field. However, we find that charged impurities in the underlying substrate cause substantial spatial fluctuation of the gap size. Our work elucidates the microscopic behavior of trilayer graphene and its consequences for macroscopic devices.

PACS numbers: 73.22.Pr, 73.21.Ac, 68.37.Ef

* leroy@physics.arizona.edu

Graphene has great potential to be used in novel electronics applications [1] due to its extraordinarily rich physical properties [2–5]. Many of these applications require inducing a sizeable band gap without sacrificing its high intrinsic carrier mobility [6]. While this has thus far not been achieved in single layer graphene, multilayer graphene has the possibility of an electric field tunable band gap. Trilayer graphene exhibits two natural stacking orders, Bernal and rhombohedral. The more commonly found Bernal-stacked trilayer graphene is not expected to exhibit a significant field tunable band gap due to its mirror symmetry [1, 2, 7, 8, 10, 12–15], and experimental evidence thus far has supported this [16–18]. Its zero-field low energy band structure behaves roughly like a decoupled stack of Bernal-stacked bilayer graphene and single layer graphene [1, 2, 7, 8, 10, 12–15]. However, rhombohedrally-stacked trilayer graphene behaves differently in an electric field owing to its lack of inversion symmetry. In this case, the low energy bands mimic a single sheet of Bernal-stacked bilayer graphene, and as such, a large field tunable band gap is expected in ABC trilayer graphene [4, 8, 12–15, 20]. Prior work has explored the zero-field band structure of this material via electrical transport measurements and found a small band gap opened due to many-body effects [21]. The magnitude of the band gap in a tunable electric field has also been studied optically [22]. However, direct spectroscopic confirmation of the electronic properties of ABC trilayer with independent control of the Fermi energy and electric field has thus far been lacking.

In this letter, we present scanning tunneling microscopy (STM) and scanning tunneling spectroscopy (STS) measurements of dual gated exfoliated samples of both ABA- and ABC-stacked trilayer graphene on Si/SiO_2 substrates. Our results provide a direct understanding of the behavior of the band gap of ABC trilayer graphene in an electric field, and illuminate the effects of local disorder on its electronic properties.

Trilayer graphene flakes were mechanically exfoliated on a SiO_2 substrate. Cr/Au electrodes were written using electron beam lithography. The devices were annealed at 350 °C for 2 h in a mixture of argon and hydrogen and then at 300 °C for 1 h in air before being transferred to the ultrahigh vacuum low-temperature STM for topographic and spectroscopic measurements. Figure 1(a) shows a schematic diagram of the measurement set-up used for imaging and spectroscopy of the trilayer graphene flakes. The layer number and stacking order of each flake was characterized using confocal Raman spectroscopy mapping prior to electrode deposition. Representative Raman signals for both stacking orders are shown in

Fig. 1(c). ABA stacked trilayers show a nearly symmetric 2D peak while ABC stacked trilayers show an asymmetric peak [21–24]. Only flakes exhibiting homogenous stacking order were used to ensure that local STM measurements were made on a known stacking order. The insets to Fig. 1(c) show spatial maps of the FWHM of the 2D peaks for an ABA- and ABC-stacked sample, indicating that the flakes have a uniform stacking order.

All the STM measurements were performed in ultrahigh vacuum at a temperature of 4.5 K. dI/dV measurements were acquired by turning off the feedback circuit and adding a small (5 mV) a.c. voltage at 563 Hz to the sample voltage. The current was measured by lock-in detection. Topographically, we measure a triangular lattice in both types of trilayer graphene samples, as illustrated for ABC trilayer graphene in Fig. 1(d), which is consistent with the expected topography for a multilayer graphene sample.

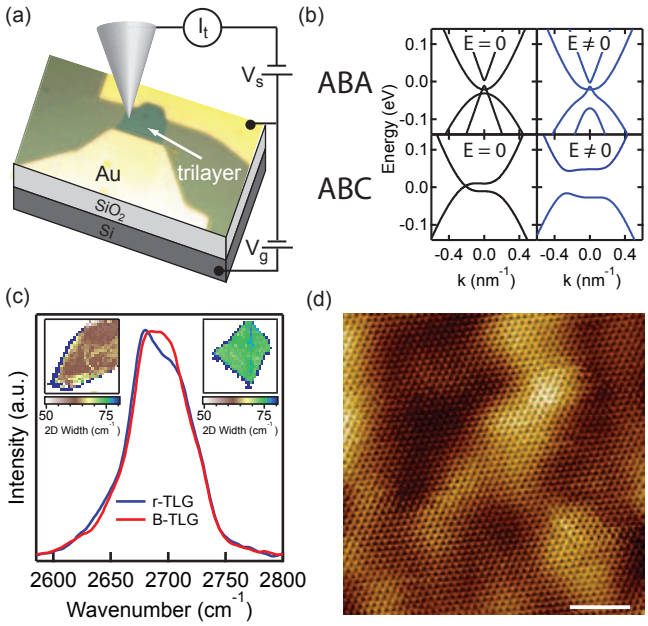

FIG. 1. (color online) Density of states of ABA and ABC trilayer graphene at varying gate voltage. (a) Schematic of the measurement setup showing the STM tip and an optical microscope image of one of the measured samples. (b) Band structure for ABA and ABC trilayer graphene with no electric field and a moderately sized electric field. (c) Raman spectroscopy of both stacking orders of trilayer graphene. Left upper inset: Map of the FWHM of the 2D peak for an ABA-stacked flake. Right upper inset: Map of the FWHM of the 2D peak for an ABC-stacked flake. (d) STM topography image of ABC trilayer graphene showing the triangular lattice. Scale bar is 2 nm. Imaging parameters were sample voltage -200 mV and tunneling current 100 pA.

We achieve dual control of the Fermi energy and perpendicular electric field by tuning the voltage on the silicon back gate and STM tip. The applied electric field is a superposition of four fields: the field due to the voltage applied to the back gate, the field due to the voltage applied to the tip, the field due to the intrinsic charged impurities in the SiO_2, and the field due to the work function difference between the graphene and the tungsten tip. Application of an electric field serves to open a band gap for the ABC-stacked trilayer graphene, as shown schematically in Fig. 1(b), while the ABA-stacked trilayer remains metallic. Figs. 2 (a) and (b) show dI/dV spectroscopy, which is proportional to the local density of states (LDOS), as a function of sample voltage and gate voltage for the ABA- and ABC-stacked trilayers respectively. Each curve is the average of 100 measurements over a 20 nm by 20 nm region. For both stacking orders, features move more positive in sample voltage as the gate voltage becomes more negative, due to the shifting of the Fermi energy. However, we also apply a larger perpendicular electric field as the gate voltage becomes more negative. For the ABA-stacked trilayer graphene in Fig. 2(a), we see two peaks separated by roughly 30 meV (as well as a dip which remains pinned to zero energy). These peaks, marked by black and white arrows, move in parallel with changing gate voltage, which suggests they are relatively insensitive to the magnitude of the electric field at the densities we probe. We calculate the band structure of ABA-stacked trilayer graphene using the low energy Hamiltonian [2, 10] and find relatively good agreement for the evolution of our features with electric field. Our calculation shows that while the single-layer like bands move farther from the Fermi energy with increasing field, the bilayer-like bands stay roughly evenly spaced and exhibit a fairly flat band edge which results in our measured peaks [25].

For the remainder of this study, we focus on the spectroscopic results for the ABC-stacked trilayer graphene, where we open a field tunable band gap. For the ABC-stacked trilayer graphene in Fig. 2(b), we see a dip in the LDOS which grows in width as the gate tunes the center of the dip away from the Fermi energy (which occurs around $V_g = +25$ V). We attribute this dip to an electric field induced band gap (gap edges marked by black tick marks). We also see a peak just above the conduction band edge which does not appear on the valence band side (marked with black arrows). This peak is a signature of the van Hove singularity at the band edge, and grows in strength as the field becomes larger and the band becomes flatter. This electron-hole asymmetry is present in all samples measured, but cannot be explained by the low energy Hamiltonian [4] and is not currently understood.

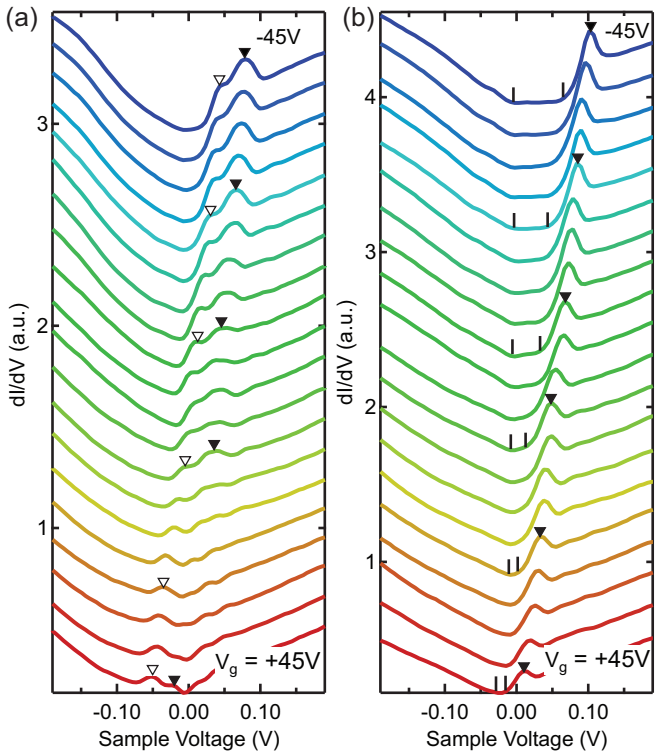

FIG. 2. (color online) Density of states of ABA and ABC trilayer graphene at varying gate voltage. (a) Experimental dI/dV curves for ABA trilayer graphene taken in regular intervals of back gate voltage between +45 V and -45 V. Black arrows indicate the location of the bilayer-like conduction band edge. White arrows indicate the location of the bilayer-like valence band edge. (b) Experimental dI/dV curves for ABC trilayer graphene taken in regular intervals of back gate voltage between +45 V and -45 V. Black arrows indicate the location of the conduction band van Hove singularity. Black tick marks represent the band gap edges. All curves are the average of 100 measurements taken over a 20 nm by 20 nm range. All curves are offset for visual clarity.

All samples measured showed considerable spectroscopic variation between locations separated on the nanometer scale. To counteract this effect, we recorded dI/dV spectroscopy curves every two nanometers over a 50 nm x 50 nm region for a variety of voltages on the back gate. We then averaged the curves before analyzing the gap size. By averaging the dI/dV spectroscopy over even a small region of the sample, we average over spatial variations in the band gap due to the varying local electric field strengths resulting from charged impurities in the underlying SiO_2 substrate. To understand the magnitude of this effect, we recorded the LDOS at a given gate voltage with higher spatial resolution over roughly the

same spatial range. We determined the energy of a given feature for each curve; we chose the van Hove singularity for the ABC-stacked trilayer graphene since this feature is the sharpest. Fig. 3(a) shows the energy of the van Hove singularity for each spectroscopy curve in a 40 nm x 40 nm region of the sample with the Fermi energy tuned near the charge neutrality point (CNP). Similar to the case of single [26–28] and bilayer graphene [29, 30], we notice spatially coherent puddles of charge on the sample which have no significant correlation with topographic features. Fig. 3(b) shows a histogram of the energy of the van Hove singularity, from which we see a roughly Gaussian distribution with a FWHM of 10.7 ± 0.8 meV. Similar measurements on different spots on the same sample, and from different samples, give comparable charge variations. We do not find significant changes in the charge variation as a function of back gate voltage, which is to be expected given that the low energy bands do not change in curvature much with changing energy and electric field. By auto-correlating the charge puddle map, we are able to estimate a puddle size of 8 ± 0.2 nm for this sample spot, as shown in Fig. 3(c).

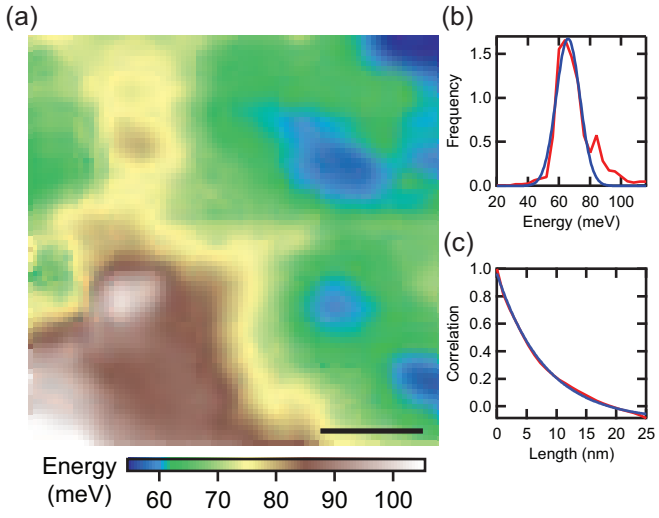

FIG. 3. (color online) Charge fluctuation map for ABC trilayer graphene. (a) Experimental dI/dV puddle map for ABC trilayer graphene taken at $V_g = +30$ V. The color scale represents the sample voltage of the van Hove singularity of the conduction band. The scale bar is 10 nm. (b) Histogram of the sample voltage values from the dI/dV puddle map. The red curve is the experimental data, and the blue curve is a best fit Gaussian. (c) Auto-correlation of the dI/dV puddle map. The red curve is the experimental data, and the blue curve is a best fit exponential.

At high induced charge density, puddles of increased charge density give larger electric

fields and hence larger band gaps. On the other hand, puddles of reduced charge density have lower electric fields and hence smaller band gaps. Given a typical puddle size of less than 10 nm, we would expect to have more than 25 puddles in our 50 nm x 50 nm scan windows. Consequently, averaging all the curves for a map taken with a high induced charge density (large electric field) will likely exhibit a gap size corresponding to the average electric field of the map, because spectroscopy curves taken in spots with larger than average charge densities are compensated for by curves taken in spots with smaller than average charge densities. However, this does not hold true for maps taken near the minimum applied electric field (near zero charge density). For both positively and negatively charged puddles, the local electric field is larger since more charges of either sign induce a bigger field, so the gap size for each individual curve can only be larger than the expected gap size given the average electric field of the map. Therefore, by averaging over many puddles, at low charge density we expect a larger gap size than anticipated.

To extract band gap sizes, we adopt a fitting procedure in which we fit a V-shaped curve separated by a horizontal line to the region directly surrounding the minimum in the LDOS [25]. The gap size is equal to width of the horizontal line. The gray circles in Figs. 4 (a) and (b) represent the gaps extracted from averaging 625 spectroscopy curves taken at each gate voltage. To further explore the potential effects of charge puddles on the gap size, we also average our data over a smaller spatial area. The exact size of this area does not qualitatively change our interpretation of the data [25]; therefore we present our results for a mesh size of 16 nm x 16 nm, which should contain no more than a few puddles. Within each of the nine subsections of a 50 nm x 50 nm map, we average all the curves within the subsection then fit a gap to that averaged curve. The colored squares in Fig. 4(a) show the fitted gap size as a function of gate voltage, where each color corresponds to a different 16 nm x 16 nm area. This data is in good agreement with the averaged data for the entire map, with both showing a gap opening on either side of the CNP at around +25 V on the back gate. The back gate serves to both tune the Fermi energy and apply an electric field, so the observed behavior is to be expected given that when the gate tunes the Fermi energy to the CNP, it also tunes the total electric field near its minimum. We measure an electric field induced gap as large as 70 meV at negative back gate voltages and as small as 15 meV near the CNP. The inset of Fig. 4(a) plots the energy of the conduction and valence band edges as a function of back gate voltage. From this, as well as from Fig. 2(b), we see that the

majority of the gap opening is due to movement of the conduction band edge. The valence band edge appears roughly pinned to zero sample voltage for back gate voltages far away from the CNP. Both band edges move roughly in parallel when the back gate is tuned close to the CNP, as the gap is small there and the Fermi energy is no longer pinned near one band. If we were able to tune our device to higher electron densities, we would expect to see the conduction band edge pinned near the Fermi energy.

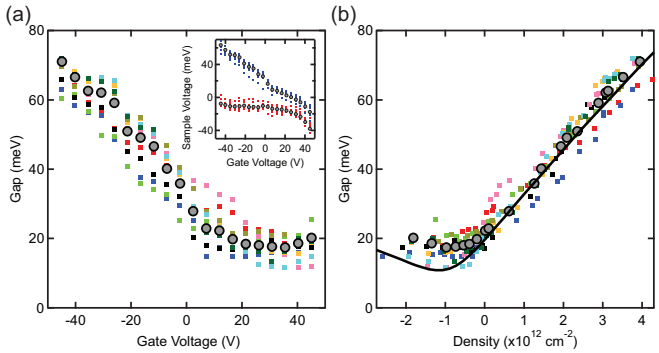

FIG. 4. (color online) Experimental and theoretical band gap size in ABC trilayer graphene as a function of back gate voltage and charge density. (a) Experimental gap size for ABC trilayer graphene as a function of back gate voltage. Gray circles represent an average of 625 measurements over a 50 nm by 50 nm range. Colored squares represent an average of 64 measurements over a 16 nm by 16 nm range. All data represented in the colored squares is within the 50 nm by 50 nm range represented by the gray circles. Statistical error bars are smaller than marker sizes. Inset: Sample voltage of the valence (red squares) and conduction (blue squares) band edges as a function of back gate voltage. Gray circles and colored squares have the same meaning as in the main figure. (b) Experimental gap size for ABC trilayer graphene as a function of charge density. All color conventions are identical to (a). The black curve is the theoretically expected gap size as a function of charge density.

We note that our conduction band edge moves at a rate of roughly 1 meV in sample voltage for every 1 V on the back gate. We use this to relate the gate voltage to induced charge density. Fig. 4(b) shows the gap sizes from Fig. 4(a) re-plotted against charge density, where zero density corresponds to a gap centered at zero sample voltage. This should account for charge puddle fluctuations, and as a result the gap sizes from different spatial locations have less variation. The solid black line represents the theoretically expected band gap size

as a function of charge density. This was calculated using the low energy Hamiltonian of ABC graphene which accounts for trigonal warping terms and interlayer screening [4]. We also add a constant charge density offset due to the work function mismatch between the tip and the trilayer graphene. For this device, the global CNP was greater than our range of back gate voltages (± 45 V), but the local CNP was around $V_g = +25$ V, so there was at least a 20 V offset due to the work function mismatch between the tip and graphene [25]. We note that this offset cannot be explained by local charge fluctuations alone, given that we see a charge variation corresponding to only about 10 V of back gate. When we account for this work function mismatch, we find theoretically that we are unable to close the band gap for any back gate voltage. Furthermore, the minimum theoretical gap is larger than the expected zero-field gap of roughly 6 meV [21] opened due to electron-electron interactions, therefore we safely ignore contributions to the band gap due to many-body effects. We see very good agreement in both the slope and magnitude of our band gap at high carrier density. At low density, we measure slightly larger than predicted gaps. Again, this is likely due to the remaining charge variation within our fine mesh. We see that some gaps are larger than predicted by as much as about 10 meV, which is to be expected if the data is averaged over a few puddles. We note that in cases where a block of data corresponds to one large puddle, such as the light blue dots, the experimentally measured gaps are very close to the theoretically expected values over all densities probed.

We have presented local spectroscopic measurements of both the ABA- and ABC- stacked trilayer graphene systems. We find that both interlayer screening and relative work function difference between the top gate and graphene play an important role in determining the magnitude of the band gap in the ABC trilayer. Finally, we see that local charge fluctuations strongly modify the size of the band gap, implying the need to control these if a controlled global gap is to be realized.

ACKNOWLEDGMENTS

The work at Arizona was partially supported by the U. S. Army Research Laboratory and the U. S. Army Research Office under contract/grant number W911NF-09-1-0333 and the National Science Foundation EECS-0925152. C.N.L. and F.W. are supported in part by

NSF CAREER DMR/0748910, NSF/1106358 and the FENA Focus Center.

---

[1] K. S. Novoselov, V. I. Fal'ko, L. Colombo, P. R. Gellert, M. G. Schwab, and K. Kim, Nature **490**, 192 (2012).

[2] K. S. Novoselov, A. K. Geim, S. V. Morozov, D. Jiang, M. I. Katsnelson, I. V. Grigorieva, S. V. Dubonos, and A. A. Firsov, Nature **438**, 197 (2005).

[3] Y. Zhang, Y.-W. Tan, H. L. Stormer, and P. Kim, Nature **438**, 201 (2005).

[4] A. H. Castro Neto, F. Guinea, N. M. R. Peres, K. S. Novoselov, and A. K. Geim, Rev. Mod. Phys. **81**, 109 (2009).

[5] S. Das Sarma, S. Adam, E. H. Hwang, and E. Rossi, Rev. Mod. Phys. **83**, 407 (2011).

[6] F. Schwierz, Nature Nanotech. **5**, 487 (2010).

[7] F. Guinea, A. H. Castro Neto, and N. M. R. Peres, Phys. Rev. B **73**, 245426 (2006).

[8] M. Aoki and H. Amawashi, Solid State Commun. **142**, 123 (2007).

[9] M. Koshino, and E. McCann, Phys. Rev. B **79**, 125443 (2009).

[10] A. A. Avetisyan, B. Partoens, and F. M. Peeters, Phys. Rev. B **79**, 035421 (2009).

[11] A. A. Avetisyan, B. Partoens, and F. M. Peeters, Phys. Rev. B **80**, 195401 (2009).

[12] M. Koshino, Phys. Rev. B **81**, 125304 (2010).

[13] S. B. Kumar and J. Guo, Appl. Phys. Lett. **98**, 222101 (2011).

[14] B.-R. Wu, Appl. Phys. Lett. **98**, 263107 (2011).

[15] K. Tang, R. Qin, J. Zhou, H. Qu, J. Zheng, R. Fei, H. Li, Q. Zheng, Z. Gao, and J. Lu, J. Phys. Chem. C **115**, 9458 (2011).

[16] M. F. Craciun, S. Russo, M. Yamamoto, J. B. Oostinga, A. F. Morpurgo, and S. Tarucha, Nature Nanotech. **4**, 383 (2009).

[17] T. Taychatanapat, K. Watanabe, T. Taniguchi, and P. Jarillo-Herrero, Nature Phys. **7**, 621 (2011).

[18] E. A. Henriksen, D. Nandi, , and J. P. Eisenstein, Phys. Rev. X **2**, 011004 (2012).

[19] A. A. Avetisyan, B. Partoens, and F. M. Peeters, Phys. Rev. B **81**, 115432 (2010).

[20] F. Zhang, B. Sahu, H. Min, and A. H. MacDonald, *Phys. Rev. B* **82**, 035409 (2010).

[21] W. Bao, L. Jing, J. Velasco Jr, Y. Lee, G. Liu, D. Tran, B. Standley, M. Aykol, S. B. Cronin, D. Smirnov, M. Koshino, E. McCann, M. Bockrath, and C. N. Lau, Nature Phys. **7**, 948 (2011).

[22] C. H. Lui, Z. Li, K. F. Mak, E. Cappelluti, and T. F. Heinz, Nature Phys. **7**, 944 (2011).

[23] C. H. Lui, Z. Li, Z. Chen, P. V. Klimov, L. E. Brus, and T. F. Heinz, Nano Lett. **11**, 164 (2011).

[24] L. Zhang, Y. Zhang, J. Camacho, M. Khodas, and I. Zaliznyak, Nature Phys. **7**, 953 (2011).

[25] See Supplementary Material at [URL will be inserted by publisher] for calculations of trilayer band structures, explanation of band gap fitting procedure, and analysis of varying mesh size.

[26] J. Martin, N. Akerman, G. Ulbricht, T. Lohmann, J. H. Smet, K. Von Klitzing, and A. Yacoby, Nature Phys. **4**, 144 (2008).

[27] A. Desphande, W. Bao, F. Miao, C. N. Lau, and B. J. LeRoy, Phys. Rev. B **79**, 205411 (2009).

[28] Y. Zhang, V. W. Brar, C. Girit, A. Zettl, and M. F. Crommie, Nature Phys. **5**, 722 (2009).

[29] A. Desphande, W. Bao, Z. Zhao, C. N. Lau, and B. J. LeRoy, Appl. Phys. Lett. **95**, 243502 (2009).

[30] G. M. Rutter, S. Jung, N. N. Klimov, D. B. Newell, N. B. Zhitenev, and J. A. Stroscio, Nature Phys. **7**, 649 (2011).

SUPPLEMENTARY MATERIAL

I. CALCULATION OF ABA BAND STRUCTURE

We model ABA-stacked trilayer graphene as three coupled honeycomb lattices, each with two inequivalent lattice sites. The layers have the standard Bernal-stacking scheme as described in Ref. [1]. We account for intra-layer couplings between nearest neighbors, γ_0, coupling between inequivalent lattice sites lying directly above and below each other, γ_1, nearest-layer coupling between the next closest set of lattice sites, γ_3 and γ_4, next-nearest-layer coupling between equivalent lattice sites, γ_2 and γ_5, and the on-site energy difference between different layer lattice sites, Δ [1]. We also account for the charge density on each layer given by n_i induced via top (n_t) and back (n_b) gating leading to potential differences between the layers. As such, we adopt the low energy Hamiltonian of Ref. [2]

$$H = \begin{pmatrix} -\Delta_{1,2}(n) + \Delta + \gamma_5 & \gamma_0 f & \gamma_1 & -\gamma_4 f^* & \gamma_5/2 & 0 \\ \gamma_0 f^* & -\Delta_{1,2}(n) + \gamma_2 & -\gamma_4 f^* & \gamma_3 f & 0 & \gamma_2/2 \\ \gamma_1 & -\gamma_4 f & \Delta + \gamma_5 & \gamma_0 f^* & \gamma_1 & -\gamma_4 f \\ -\gamma_4 f & \gamma_3 f^* & \gamma_0 f & \gamma_2 & -\gamma_4 f & \gamma_3 f^* \\ \gamma_5/2 & 0 & \gamma_1 & -\gamma_4 f^* & \Delta_{2,3}(n) + \Delta + \gamma_5 & \gamma_0 f \\ 0 & \gamma_2/2 & -\gamma_4 f^* & \gamma_3 f & \gamma_0 f^* & \Delta_{2,3}(n) + \gamma_2 \end{pmatrix}, \tag{1}$$

with $\Delta_{1,2}(n) = -\alpha|(n_2 + n_3 - n_\mathrm{b})|$ and $\Delta_{2,3}(n) = -\alpha|(n_3 - n_\mathrm{b})|$. f is defined as $f(k_\mathrm{x}, k_\mathrm{y}) = e^{ik_\mathrm{x}a_0/\sqrt{3}} + 2e^{-ik_\mathrm{x}a_0/2\sqrt{3}} \cos k_\mathrm{y}a_0/2$, with $a_0 = 2.46$ Å the length of the in-plane lattice vector. We take $\alpha = e^2c_0/\epsilon_0\kappa$ with $c_0 = 3.35$ Å the interlayer distance and $\kappa = 2.3$ the dielectric screening constant corresponding to graphene layers on SiO_2. We take $\gamma_0 = 3.12$ eV, $\gamma_1 =$ 0.377 eV, $\gamma_2 =$ -0.0206 eV, $\gamma_3 = 0.29$ eV, $\gamma_4 = 0.12$ eV, $\gamma_5 = 0.025$ eV, and $\Delta =$ -0.009 eV [3]. Our sign convention differs slightly from Ref. [2] for overall consistency.

We model our silicon back gate as a parallel plate capacitor capable of inducing a density $n_\mathrm{b} = \alpha_g(V_\mathrm{g} - V_0)$, where $\alpha_g = 7.19$ x $10^{10}\mathrm{cm}^{-2}$ V^{-1} is determined by the gate capacitance with 300 nm of SiO_2, V_g is the applied gate voltage and V_0 is the shift of the charge neutrality point (CNP) due to intrinsic doping. Similarly, we model our tip as a parallel plate capacitor with an effective distance of 1 nm. We also add a constant density offset to the tip to account for the work function difference between the tip and trilayer graphene.

For ABA graphene and a tungsten tip, we estimate this to be equivalent to -10 V on the back gate, as this was the approximate difference between the global and local CNP. Combining these effects, we estimate our tip induced density as a function of back gate induced density as $n_{\rm t} = -0.07 n_{\rm b} - \alpha_g V_{\rm offset}$, where $V_{\rm offset}$ is the effective back gate voltage due to the work function mismatch. We use this, as well as the self-consistent screening calculations from Ref. [2], to define the layer densities as $n_2 = 0.3(n_{\rm b} + n_{\rm t})$ and $n_3 = 0.58 n_{\rm b} + 0.1 n_{\rm t}$.

Fig. S1(a) shows a numerical calculation of the density of states as a function of charge density, where darker colors represent lower density of states. A linear shifting of the Fermi energy caused by the induced charge from the back gate is not included in this calculation. The main features to notice are two spikes surrounding the minimum in the density of states. These spikes originate from the van Hove singularities of the bilayer-like bands. They are separated by about 25 meV, and their relative separation only weakly depends on the charge density. We therefore attribute our two peaks in Fig. 2(b) of the main text to the van Hove singularities of the bilayer-like bands. The dark region roughly surrounding -25 meV in sample voltage has a non-zero density of states, and thus we expect ABA trilayer graphene to remain metallic.

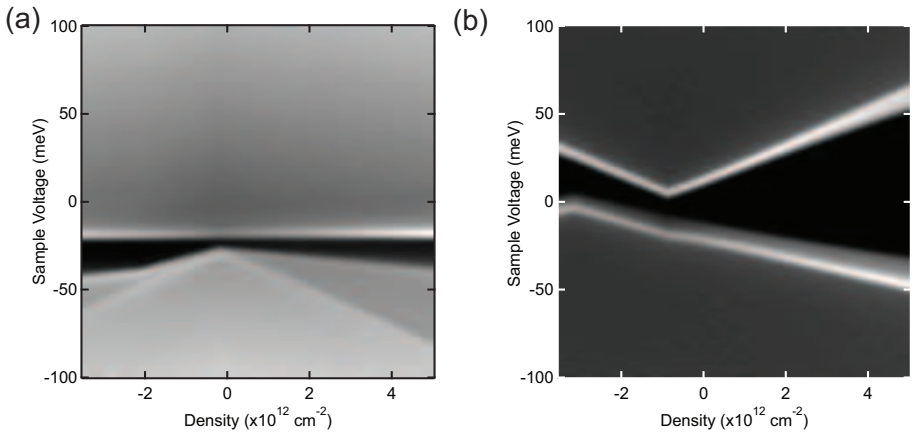

FIG. S1. Density of states simulations for ABA and ABC trilayer graphene. (a) Calculated density of states for ABA trilayer graphene. (b) Calculated density of states for ABC trilayer graphene. Darker color represents lower density of states. Both calculations include a work function offset due to the tungsten STM tip.

II. CALCULATION OF ABC BAND STRUCTURE

Similarly to the case of ABA-stacked trilayer graphene, we model ABC-stacked trilayer graphene as three coupled honeycomb lattices, each with two inequivalent lattice sites. The layers have the standard rhombohedral-stacking scheme as described in Ref. [4]. We account for the couplings described for the ABA-stacked trilayer appropriate for the ABC-stacked trilayer and adopt the low energy Hamiltonian of Ref. [4]

$$H = \begin{pmatrix} \Delta_{1,2}(n) & \gamma_0 f & \gamma_1 & -\gamma_4 f^* & 0 & 0 \\ \gamma_0 f^* & \Delta_{1,2}(n) & -\gamma_4 f^* & \gamma_3 f & 0 & \gamma_2/2 \\ \gamma_1 & -\gamma_4 f & 0 & \gamma_0 f & -\gamma_4 f^* & \gamma_3 f \\ -\gamma_4 f & \gamma_3 f^* & \gamma_0 f^* & 0 & \gamma_1 & -\gamma_4 f^* \\ 0 & 0 & -\gamma_4 f & \gamma_1 & -\Delta_{2,3}(n) & \gamma_0 f \\ 0 & \gamma_2/2 & \gamma_3 f^* & -\gamma_4 f & \gamma_0 f^* & -\Delta_{2,3}(n) \end{pmatrix}, \tag{2}$$

where all parameters in Eqn. 2 are defined as in the prior section.

For our sample presented in the main text, we estimate the work function difference to be equivalent to -25 V on the back gate. This is an educated guess, since we were unable to directly probe the global CNP. However, prior ABC trilayer samples, where both the global and local CNPs were accessible, showed similar work function mismatches. Furthermore, changing this offset corresponds to a small horizontal shift of the black curve from Fig. 4(b) of the main text, and does not qualitatively change our interpretation of the results. Again, we use this along with the self-consistent screening calculations from Ref. [4] to define the layer densities as $n_2 = 0.2(n_\mathrm{b} + n_\mathrm{t})$ and $n_3 = 0.6n_\mathrm{b} + 0.2n_\mathrm{t}$.

Fig. S1(b) shows the same density of states calculation as in Fig. S1(a), but for ABC-stacked trilayer graphene. Again, the linear shifting of the Fermi energy due to the back gate is not included in the calculation. The dark region roughly surrounding 0 meV in sample voltage has exactly zero density of states and represents the band gap. We extract the theoretical magnitude of the indirect band gap as a function of charge density from this calculation.

III. FITTING OF BAND GAPS

We fit the band gap using a piecewise defined function given by

$$f(x) = \begin{cases} A(x - valence) + B & \text{for } x \leq valence \\ B & \text{for } valence < x < conduction \\ C(x - conduction) + B & \text{for } x \geq conduction \end{cases} \tag{3}$$

where A, B, C, *valence*, and *conduction* are fit parameters. The gap size is the energy separation between the *valence* and *conduction* parameters. We also add the constraint that B must be equal to the minimum value of dI/dV (i.e. the gap minimum). Finally, we only fit this function over a small range around the gap to avoid influences from the different slopes in dI/dV around the van Hove singularity in the conduction band side. The red curve in Fig. S2(a) shows an example of a dI/dV curve at V_g = +45 V averaged over a 50 nm by 50 nm region. The blue curve is the best fit of the dI/dV curve using our gap fit function. Fig S2(b) shows similar results for V_g = -45 V.

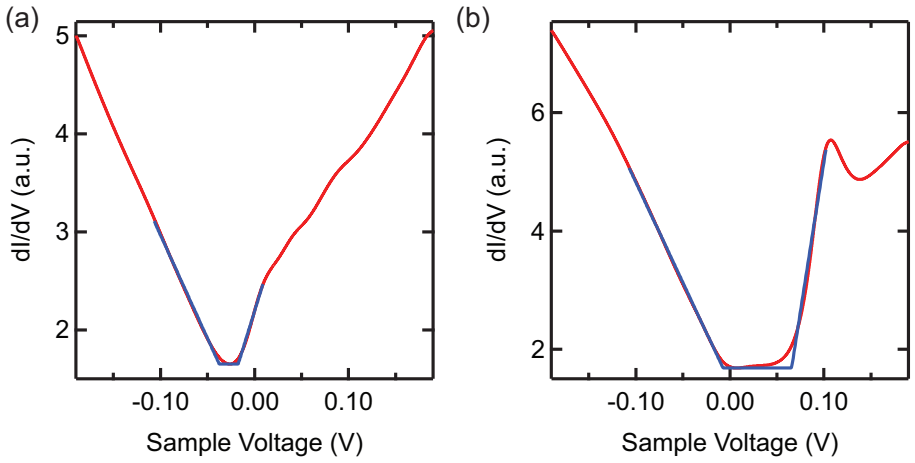

FIG. S2. Example best fit gap determination curves at different back gate voltages. (a) The red curve is the average of 625 spectroscopy curves from the same data set as the main text at V_g = +45 V. The blue curve is the best fit using our gap function and is only plotted over the fitted region of data. (b) Same as (a), but for V_g = -45 V.

IV. VARYING MESH SIZE

We do not see qualitative changes in the gap fits as a function of mesh size. Smaller mesh sizes give the advantage of less charge variation for each set of curves, but come at the expense of fewer curves to average. Conversely, larger mesh sizes offer more curves to average but come at the expense of averaging over more charge fluctuations. Fig. S3 shows the same analysis as in Fig. 4(b) of the main text, but using a mesh size of 10 nm by 10 nm. The gray circles and solid black curve are the same is in Fig. 4(b) of the main text. The solid blue dots are the fits for the local gap size as a function of charge density. There is a larger spread in gap size at a given charge density for the smaller mesh size, but the overall magnitude and trend of the data as a function of charge density remains the same as for the larger mesh size. Outlier points are the results of bad spectroscopy curves, which get averaged away with larger mesh sizes.

---

[1] M. Koshino, and E. McCann, Phys. Rev. B **79**, 125443 (2009).

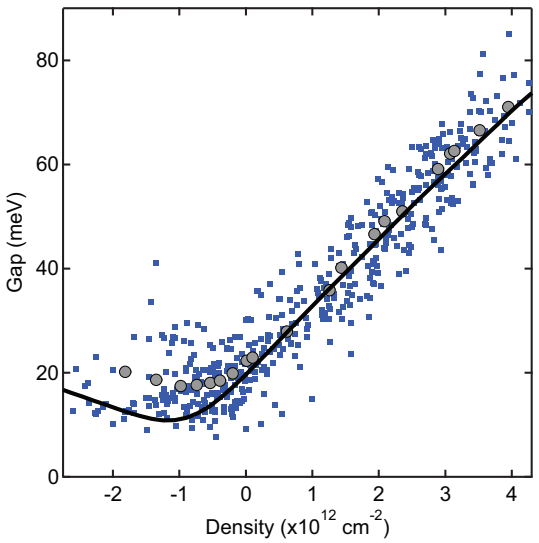

FIG. S3. Experimental and theoretical band gap size in ABC trilayer graphene as a function of charge density. The gray circles and black curve are the same as in Fig. 4(b) of the main text. The blue dots represent the experimental best fit gap size for the same data is in Fig. 4 of the main text, but with a mesh size of 10 nm by 10 nm.

[2] A. A. Avetisyan, B. Partoens, and F. M. Peeters, Phys. Rev. B **80**, 195401 (2009).

[3] B. Partoens and F. M. Peeters, Phys. Rev. B **74**, 075404 (2006).

[4] A. A. Avetisyan, B. Partoens, and F. M. Peeters, Phys. Rev. B **81**, 115432 (2010).